SO_3 decomposition over $CuO–CeO_2$ based catalysts in the sulfur–iodine cycle for hydrogen production

Lijian Wang[1], Yanqun Zhu[1], Hui Yang[1], Yong He[1,*], Jun Xia[2,*], Yanwei Zhang[1], Zhihua Wang[1]

[1]*State Key Laboratory of Clean Energy Utilization, Zhejiang University, Hangzhou 310027, China*
[2]*Department of Mechanical, Aerospace and Civil Engineering, Brunel University London, Uxbridge UB8 3PH, UK*

*Corresponding author: heyong@zju.edu.cn, Jun.Xia@brunel.ac.uk

Abstract

The effect of several catalyst supports with large specific surface area (such as SiC, Al_2O_3, $SiC–Al_2O_3$–ball, and $SiC–Al_2O_3$) on catalytic activity was evaluated in this study. $CuO–CeO_2$ supported on $SiC–Al_2O_3$ exhibited high stability and activity, which was considerably close to the thermodynamic equilibrium curve at 625 °C during the stability test for 50 h. The SO_3 decomposition temperature decreased from 750 °C to 625 °C. $SiC–Al_2O_3$contained numerous micropores and mesopores and had a large specific area, indicating strong adsorption, as determined by transmission electron microscopy (TEM), high-resolution transmission electron microscopy (HRTEM), X-ray diffraction (XRD), and nitrogen adsorption measurement. X-ray photoelectron spectroscopy (XPS) revealed that the surface of $SiC–Al_2O_3$consisted of Al_2O_3, SiC, and SiO_2 and that the cerium oxide surface had the largest number of defects. Temperature-programmed reduction (H_2-TPR) results indicated that the cerium–copper oxides on the surface of powdered $SiC–Al_2O_3$ had the strongest redox potential and that CuO had the lowest reduction temperature.

Keywords

hydrogen production; sulfur–iodine cycle; sulfuric acid decomposition; carriers of cerium–copper composite oxides

1. Introduction

Hydrogen is an important industrial feedstock that can be stored and transported, apart from its other desirable characteristics[1, 2]. The sulfur–iodine (SI) thermal chemical cycle can be potentially used in large-scale hydrogen production through water splitting without greenhouse gas emissions, as an alternative to steam reforming and water electrolysis. Another advantage is that the technique can easily match solar energy, renewable and nuclear energy[3, 4].Numerous studies have been conducted on the SI cycle since the proposal by General Atomics in the 1970s[5-17].

The reaction scheme of the SI cycle consists of 3 steps:

$$SO_2 + I_2 + 2H_2O \xrightarrow{20\text{-}120^oC} H_2SO_4 + 2HI \quad (1)$$

$$2HI \xrightarrow{300\text{-}500^oC} H_2 + I_2 \quad (2)$$

$$H_2SO_4 \xrightarrow{600\text{-}900^oC} SO_2 + H_2O + 1/2O_2 \quad (3)$$

The so-called Bunsen reaction [reaction (1)] refers to the reduction of iodine to hydrogen iodide and the oxidation of sulfur dioxide to sulfuric acid, producing 2 non-miscible acidic phases (HI_x and sulfuric acid phase) in the presence of excess iodine. After purification and distillation, the HI from the HI_x phase decomposed into hydrogen and iodine, as shown in reaction (2). Hydrogen is then collected, and iodine is transported back to the first step Bunsen reaction. The purified phase of sulfuric acid is decomposed into sulfur dioxide, oxygen, and water under a specific condition as shown in reaction (3). The products of the second and third reactions are delivered back to the first reaction as reactant, except for oxygen and hydrogen[18].

Reaction (3) is a strongly endothermic process, which requires temperature as high as 900 °C. It actually consists of two sub–steps, namely, reactions (4) and (5):

$$H_2SO_4(g) \xrightarrow{350-500^oC} H_2O(g) + SO_3(g) \quad (4)$$

$$SO_3(g) \xrightarrow{600-900^oC} SO_2(g) + 1/2\,O_2(g) \quad (5)$$

H_2SO_4 can be easily converted into SO_3 and H_2O at 350°C–500 °C[19]. However, in the absence of catalysts, the SO_3decomposition temperature is extremely high because of its kinetic limitations[20]. Therefore, catalytic decomposition is necessary and the most commonly used method to improve the SO_3 decomposition and decrease the needed temperature within the limitation of thermodynamic [21, 22].

The catalytic decomposition of SO_3 is substantially improved when SiO_2, TiO_2, Al_2O_3, ZrO_2, and $BaSO_4$ are used as support materials for Pt, CuO, and Fe_2O_3 catalysts[23]. However, the activities of Pt/Al_2O_3, Pt/SiO_2, CuO/SiO_2, and CuO/TiO_2 decrease with the reaction time because of the formation of sulfates. When Pt is loaded on SiC, the instability problem of Pt/Al_2O_3 can be overcome[10]. The catalytic decomposition of sulfuric acid at 650°C–850 °C for Pt/Al_2O_3 and $Pt–SiC–Al_2O_3$ has been investigated[24]. At temperature< 700 °C, Al_2O_3 can usually form into aluminum sulfate; however, on the carrier surface of the $Pt–SiC–Al_2O_3$ catalyst, sulfate or any other compound of sulfur is not detected. The high cost of Pt catalysts restricts its large-scale application. Previous study has reported that Fe_2O_3 supported on SiC is found to exhibit excellent catalytic performance[25] and the deactivation is also investigated. Complex metal oxide catalysts ($CuCr_2O_4$, Cr/Fe oxide, $CuO–V_2O_5$, and $CuO–CeO_2$) appear to be the most promising candidates replacing for Pt catalysts[26-29]. The porous catalyst Cu–V (oxide)/SiO_2 could decrease the SO_3 decomposition temperature from 800 °C to 650 °C[30-32], but its stability needs to be further verified. The $CuO–CeO_2$ complex oxide catalyst is an excellent catalyst for SO_3 decomposition[33], while the activity and stability are unsatisfactory at temperature <720 °C. CuO – CeO_2 supported on SiC, γ-Al_2O_3, and $SiC–Al_2O_3$ (widely used supports) may be suitable for the catalytic decomposition of the SO_3, but the final performance and stability are closely related to the carrier properties, which can be influenced by preparation process and composition selection.

Therefore, this research comprehensively studied the effect of different catalyst carriers to the performance of SO_3 decomposition and stability. Catalyst carriers with abundant pore structure and surface area, were selected here, such as improved γ-Al_2O_3, SiC, $SiC–Al_2O_3$–ball, and $SiC–Al_2O_3$. Characterization methods, including transmission electron microscopy (TEM), high-resolution transmission electron microscopy (HRTEM), X-ray diffraction (XRD), N_2

adsorption test, X-ray photoelectron spectroscopy (XPS), and temperature-programmed reduction (TPR), were used to analyze the structural properties of the supported cerium–copper oxide catalysts. To improve the adsorption capacity and redox activity of the catalyst and consequently decrease the SO_3 decomposition temperature, different carriers supporting cerium–copper oxide were studied using different methods.

2. Experimental methodology

2.1. Catalyst preparation

The selected carriers are identified as follows: spherical γ-Al_2O_3 (1–2mmparticle size, Gongyi Zhengda Environmental Protection Materials Co., Ltd.), spherical γ-Al_2O_3–SiC(prepared using the method described below), nano-SiC (40 nmaverage diameter, Shanghai Aladdin Biochemical Technology Co., Ltd.),and powder Al_2O_3–SiC (prepared using the method described below).

Sucrose (Sinopharm Chemical Reagent Co., Ltd.), glycol (Sinopharm Chemical Reagent Co., Ltd.), and tetraethoxysilane (Sinopharm Chemical Reagent Co., Ltd.) were dissolved in deionized water with a mole ratio of 1:4:2:40. After severe stirring, the solution was added into Al_2O_3 balls (the molar ratio of tetraethoxysilane and Al_2O_3 was 1:5). The sample was stored at room temperature for 12 h, heated to 60 °C, and kept isothermally to form a gel. Sucrose, glycol, tetraethoxysilane, and aluminum nitrate (Sinopharm Chemical Reagent Co., Ltd.) were dissolved in deionized water with a mole ratio of 3:15:7:16:600 and then stirred at 60 °C to form another gel. The 2 gels that were produced were dried at 110 °C for 24 h, sintered at 300 °C for 1 h, and calcined at 800 °C for another period of 24 h in nitrogen atmosphere. The samples were then cooled to room temperature. Subsequently, the calcined sample was further sintered at 700 °C in air for 3 h. The samples produced from the former and latter gels were marked as SiC–Al_2O_3–ball and Al_2O_3–SiC.

The catalysts (CeCu–Al_2O_3, CeCu–SiC–Al_2O_3–ball, CeCu–SiC, andCeCu–SiC–Al_2O_3) were synthesized using the sol-gel method. The molar ratio of cerium nitrate hexahydrate (Sinopharm Chemical Reagent Co., Ltd.), copper nitrate hydrate (Sinopharm Chemical Reagent Co., Ltd.), citric acid (Sinopharm Chemical Reagent Co., Ltd.), glycol, and deionized water was 5:5:20:2:80, and the components were mixed and stirred at 60 °C. After severe stirring, the carrier was added and heated. A gel was then formed. The produced gel was dried at 110 °C for 24 h, sintered at 300 °C for 1 h in air, sintered at 700 °C for another 3 h, and then cooled to room temperature. The cerium–copper oxide loading amount was 12.5 wt.%. The 4 catalysts were labeled as "CeCu–Al_2O_3," "CeCu–SiC–Al_2O_3–ball," "CeCu–SiC," and "CeCu–SiC–Al_2O_3."

2.2. Characterization

The Brunner−Emmett−Teller (BET) surface area and porosity were measured by N_2 adsorption on ASAP 2020 apparatus (Micromeritics Instrument Corporation). Each sample was degassed at 250 °C for 6 h. Powder XRD was performed using a D/max 2550PC (Panalytical Instrument Corporation) diffractometer at 40 kV and 100 mA (step time of 0.02 s and step size of 0.02º). TEM and HRTEM images were obtained on Tecnai G^2 F20 S-TWIN (FEI Company). The powders were ground and then coated on the surface of molybdenum grids with ethanol. XPS was conducted on an Escalab 250Xi system (Thermo Scientific Ltd.) with MgKα radiation under ultra-high vacuum conditions (5×10^{-8} Pa). The AutoChemII 2920 automated catalyst characterization system (Micromeritics Instrument Corporation) was used for temperature

programmed reduction (TPR).

2.3. Catalytic activity and stability testing

A schematic of the catalytic activity and stability testing apparatus is presented in Figure 1. Sulfuric acid solution (92.5wt.%, Sinopharm Group Chemical Reagent Co., Ltd.) was pumped, preheated, and carried into Furnace 1 (500 °C) by nitrogen gas, which was controlled using a mass flow meter (ALICAT) at a flow rate of 1 L/min under standard conditions. Catalysts (weighing 10 g) were loaded in a quartz tube reactor in Furnace 2. The mixed gas streams from Furnace 2 passed through a spiral condenser, 3 gas-washing bottles with a NaOH solution, a gas dryer bottle with silica gel, and finally went to an online oxygen analyzer (Repidox-1100Z, Cambridge Sensotec, Ltd).

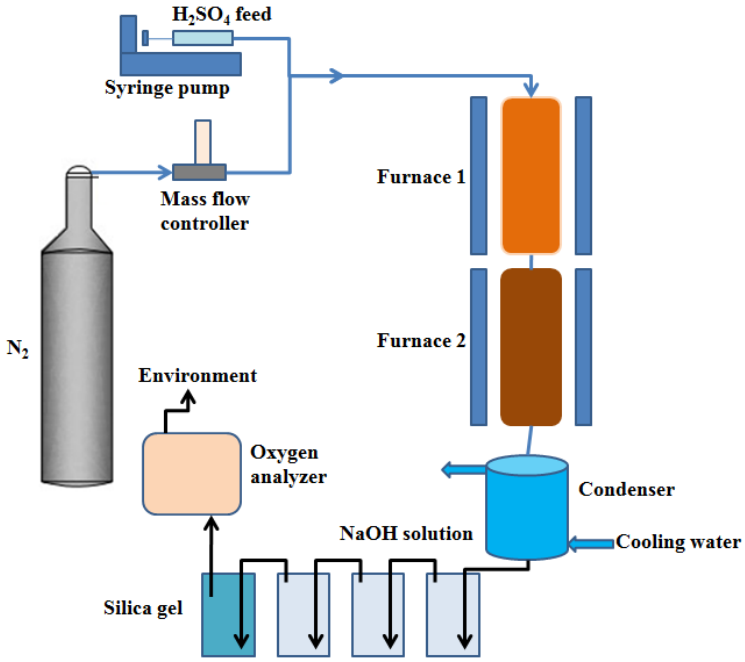

Figure 1. Testing apparatus for sulfuric acid decomposition.

3. Results and discussion

3.1. Catalytic activity

The activity of the 4 catalysts in Figure 2 (10g/$g_{catalyst}$-h weight hourly space velocity[18]) was high, particularly at > 700°C, and the SO_3 conversion ratio was close to the equilibrium decomposition limitation. At 600°C–700°C, the 4 catalysts exhibited different activities. CeCu–SiC was not active within this temperature range, and the conversion rate was 10% at 650°C. CeCu–Al_2O_3 and CeCu–SiC–Al_2O_3–ballexhibited slightly higher activities than that of CeCu–SiC, and SO_3 conversion was about 20% at 650°C.CeCu–SiC–Al_2O_3 exhibited the highest catalytic activity, and the SO_3 conversion rate at 625 °C was approximately 60%, which was close to the equilibrium decomposition rate. Figure 3 further illustrates the catalytic activity of CeCu–SiC–Al_2O_3 at different space velocities. The SO_3 conversion rate was close to the equilibrium rate at >625°C with 10 g/$g_{catalyst}$-h space velocity, as shown in Figure 3. With a further increase in space velocity to 50 g/$g_{catalyst}$-h, the catalytic conversion rate of SO_3 gradually decreased, which was apparent at 625°C–750 °C, for higher space velocity means shorter residence time[10]. The change in SO_3 conversion decreased with an increase in temperature. At

625 °C and 200 $g/g_{catalyst}$-h space velocity, the catalyst showed nearly no activation. The reason might be that when the sulfate formation rate exceeded the sulfate decomposition rate, a large amount of sulfate was formed, without enough residence time to decompose, resulting in a decrease in the SO_3 decomposition capacity of the catalyst according to the catalytic mechanism[34]. However, at the same temperature, pumping of sulfuric acid was stopped, and 1h after re-feeding, catalytic activity returned. Evidently, stable sulfate was not formed.

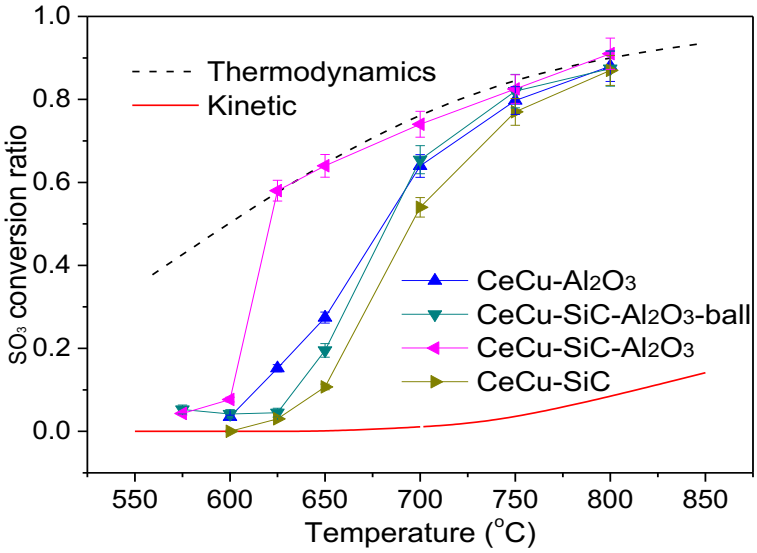

Figure 2.SO_3 conversion ratio with complex oxide catalysts supported by different carriers

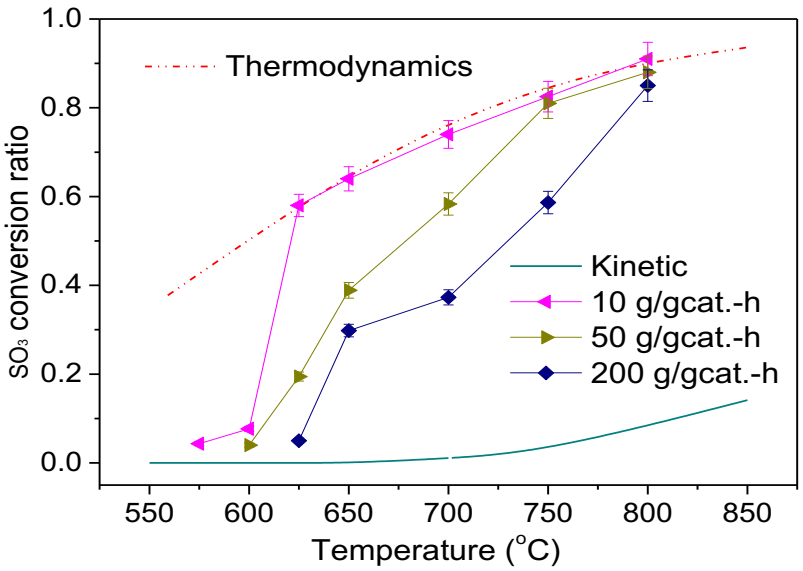

Figure3. Catalytic activity of CeCu–SiC–Al_2O_3 catalysts under different space velocities

3.2. Characterization of the catalysts

Table 1 lists the BET specific surface areas and porosities of the 4 catalysts, namely, CeCu–Al_2O_3, CeCu–SiC–Al_2O_3–ball, CeCu–SiC, and CeCu–SiC–Al_2O_3. The BET specific surface area is an important factor for catalytic activity[35, 36]. The results suggest that CeCu–SiC, which has the lowest surface area, exhibits the lowest activity, whereas CeCu–SiC–Al_2O_3, which

has the highest surface area, exhibits the highest activity. Meanwhile, CeCu–SiC–Al_2O_3 has an average pore size of 5.42 nm, which is the smallest pore size among the four. And smaller pore size may result in its higher specific surface area. It may have the highest SO_3 adsorption capacity, and its strong adsorption benefits the adsorption of the SO_3 and thus favours the decomposition reaction[36].

Table 1. Specific surface areas and porosities of CeCu–Al_2O_3, CeCu–SiC–Al_2O_3–ball, CeCu–SiC, and CeCu–SiC–Al_2O_3.

Catalyst	S_{BET} (m^2/g)	Average pore size (nm)	Pore volume (cm^3/g)
CeCu–Al_2O_3	164.56	8.11	0.33
CeCu–SiC–Al_2O_3–ball	118.09	11.68	0.34
CeCu–SiC	20.43	11.96	0.036
CeCu–SiC–Al_2O_3	170.1	5.42	0.11

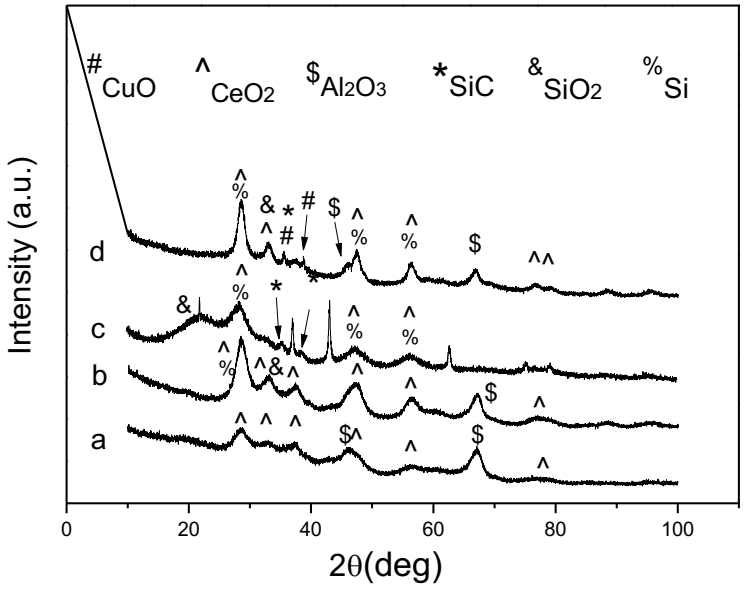

Figure 4. XRD profiles of catalysts (a) CeCu–Al_2O_3, (b) CeCu–SiC–Al_2O_3–ball, (c) CeCu–SiC, (d) CeCu–SiC–Al_2O_3.

The XRD spectra of CeCu–Al_2O_3, CeCu–SiC–Al_2O_3–ball, CeCu–SiC, and CeCu–SiC–Al_2O_3 are shown in Figure 4. CeO_2 and Al_2O_3 diffraction peaks in different directions were observed in CeCu–Al_2O_3. The SiC crystal signal peak was not detected on the surface of the CeCu–SiC–Al_2O_3–ball, compared with CeCu–SiC; however, the SiO_2 and Si diffraction peaks were detected. This finding indicated that Si and C reaction did not proceed completely during the

preparation of silicon carbide, allowing the oxidation of some SiC or Si to SiO_2 while the catalyst was burned in air. The spectrum of the CeCu–SiC catalyst showed a significant SiO_2 protrusion near the diffraction angle of 20°; thus, that the calcination temperature of 700°C also led to the apparent oxidation of SiC[18].The SiC crystal peak of the CeCu–SiC catalyst was also weak owing to the overlap of peaks. The XRD spectrum of CeCu–SiC–Al_2O_3 was mainly CeO_2, Al_2O_3, and SiC diffraction peaks, weak diffraction peaks of CuO and SiO_2. The SiC layer helps prevent support disintegration. Therefore, CeCu–SiC–Al_2O_3 can potentially exhibit high stability[24]. The XRD results showed that the cerium–copper oxide was well dispersed and immobilized on the surface of the carrier. Moreover, the apparent peak (at 28.55º) indicated abundant low-energy CeO_2 plane, which played an important role in obtaining O from adsorbed SO_3 during the decomposition reaction[33].

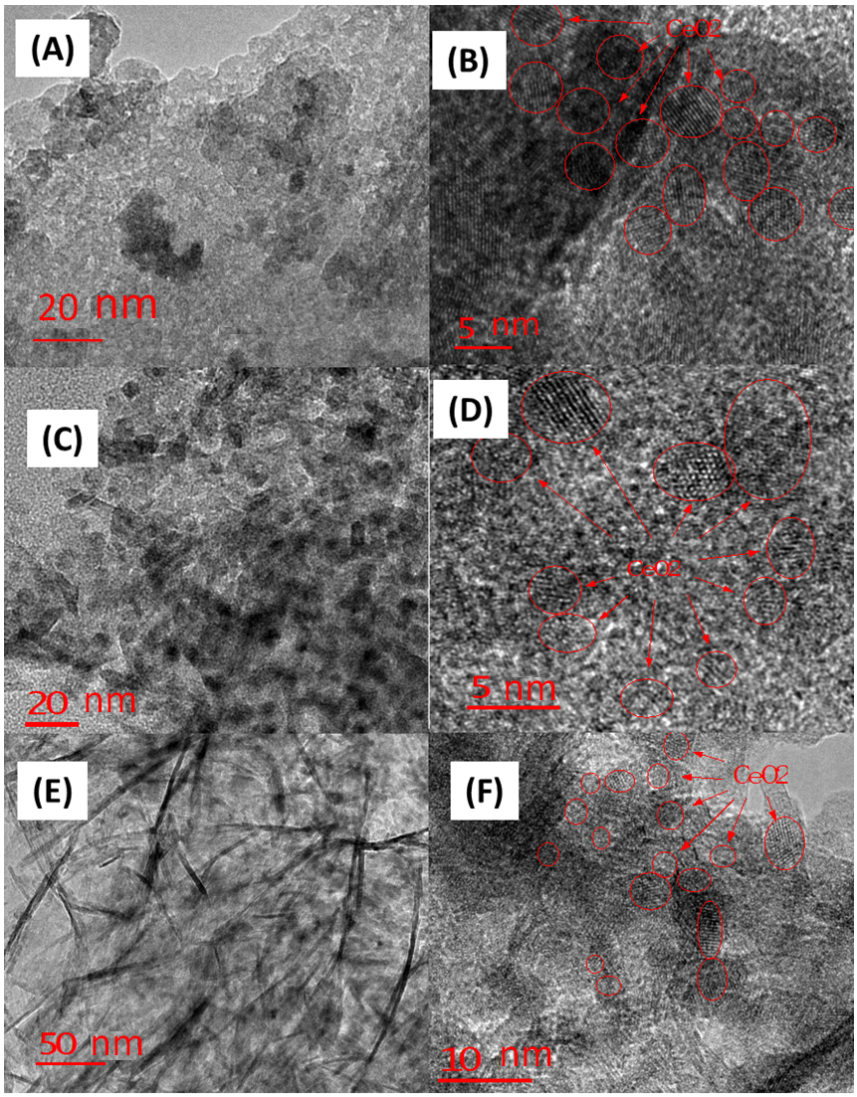

Figure 5. TEM and HRTEM images of different catalysts (ruler unit: nm), (A–B) CeCu–SiC–Al_2O_3, (C–D) CeCu–Al_2O_3, and (E–F) CeCu–SiC–Al_2O_3–ball.

Figure 5 presents the TEM and HRTEM images of the catalysts (e.g., CeCu–SiC–Al_2O_3, CeCu–Al_2O_3, and CeCu–SiC–Al_2O_3–ball). Figure 5A shows that the CeCu–SiC–Al_2O_3 has a dense surface void distribution and a large number of mesopores. As provided in Figure 5B, the

ceria with an average size of 5 nm was uniformly dispersed on the surface of SiC–Al_2O_3, and the crystal surface was clear. This finding indicated that the surface of the carrier had a less amorphous coverage and that ceria was highly dispersed, which was conducive to SO_3 adsorption for the catalytic reaction. In Figure 5C, the fragmented particle aggregates have a larger number of surface voids. This finding also led to the large specific surface area of the catalyst in Table 1. Figures 5E and 5F present a striped Al_2O_3 structure, and CeO_2 dispersion on the CeCu–SiC–Al_2O_3–ball surface.

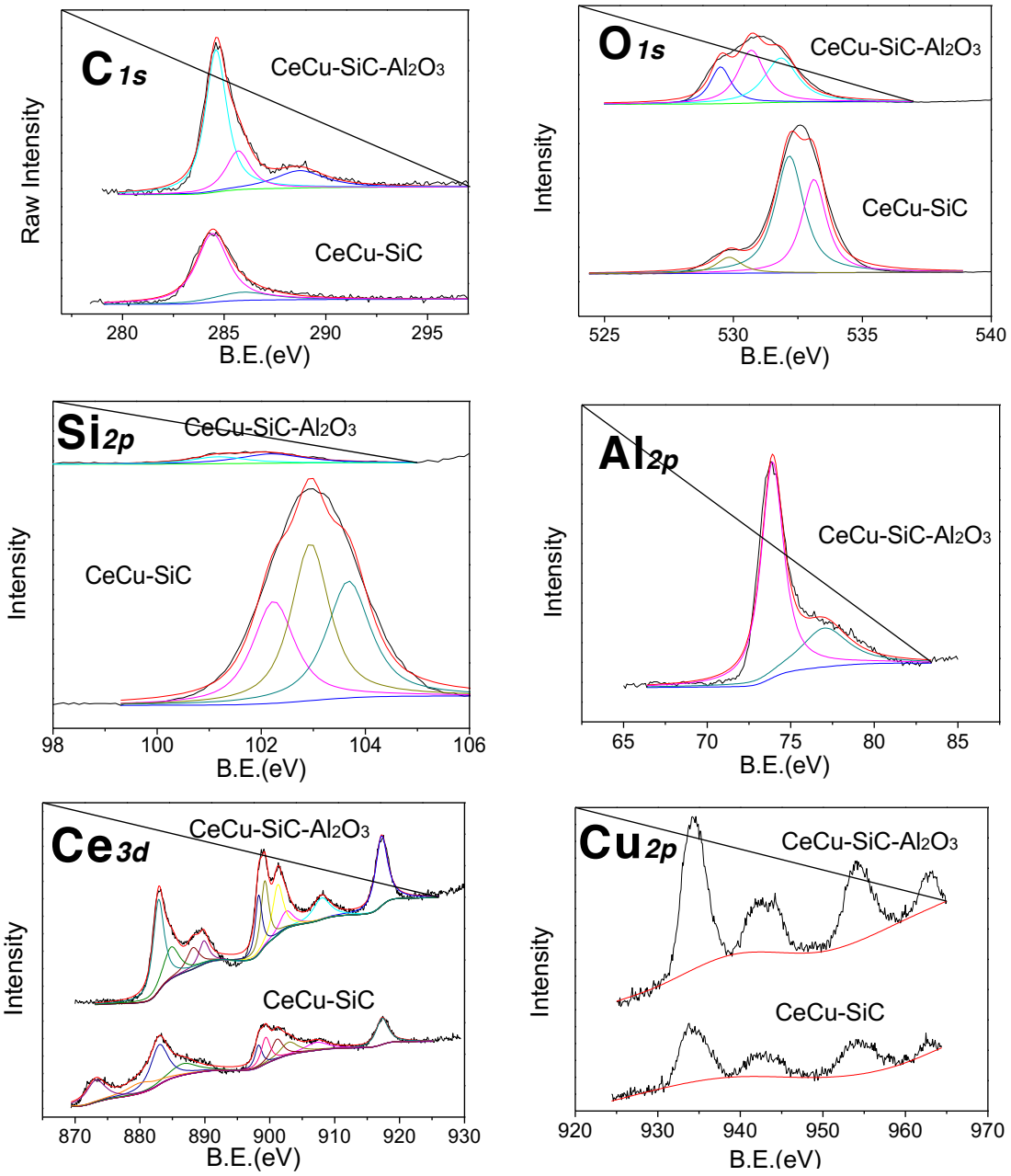

Figure 6. XPS spectra of CeCu–SiC–Al_2O_3 and CeCu–SiC.

Figure 6 demonstrates the XPS spectra of the catalysts CeCu–SiC–Al_2O_3 and CeCu–SiC. The C_{1s} peaks in CeCu–SiC–Al_2O_3 and CeCu–SiC near 283 eV are attributed to SiC[36-38]. The C_{1s} characteristic peaks of CeCu–SiC–Al_2O_3 in the vicinity of 285 eV could be attributed to the replacement of carbon from SiC matrix oxidation or carbon in the silicon–carbon reaction[37].

The binding energy position signal of the CeCu–SiC surface was not strong, indicating that the carbon signal near 285 eV might belong to a small amount of completely burned solid carbon. The peak at the junction of 289 eV represented $Si_4C_{4-x}O_2$[37], and the CeCu–SiC–Al_2O_3 signal was relatively strong.

The O_{1s} spectrum of CeCu–SiC–Al_2O_3 shows that the signal of the shoulder peak was strong near 531.2 eV (denoting an oxygen vacancy defect), indicating the presence of more active sites for SO_3 adsorption on the CeCu–SiC–Al_2O_3 surface. The peak near 529.4eV represented the lattice oxygen of cerium oxide[39]. In addition, the peak near 533eV indicated that H_2O was adsorbed on the surface of the catalyst CeCu–SiC while it overlapped with the signal peaks representing SiO_2[40]. The oxidized SiO_2 surface could be good for ceria being fixed on the SiC[18].

The Si_{2p} signal on the CeCu–SiC–Al_2O_3 surface was weak. The peak near the 101eV represented SiC, which indicated that SiC was formed on the surface of CeCu–SiC–Al_2O_3. The CeCu–SiC peak at the lower BE side (103eV) represented the combination of SiO_2 and SiC, and the peak at 104 eV indicated SiO_2 because the SiC particles on the surface were converted to amorphous SiO_2 even during calcination at 700 °C[18],which was consistent with the XRD result. The peak near 102 eV represented Si/SiO_2.

According to the strong Al_{2p} signal on the CeCu–SiC–Al_2O_3 catalyst, the signal peaks near 74and 77eV represented Al_2O_3, and the γ-Al_2O_3 ratio was higher on the surface of the catalyst, compared with the Si_{2p} spectra. The XRD pattern also showed that the catalyst phase structure was γ-Al_2O_3.

The Ce^{3+} characteristic peaks were denoted as v^0, v', u^0, and u'; all the other peaks were marked as Ce^{4+} characteristic peaks[41]. According to the results of peak analysis, the Ce^{3+}/Ce_{3d} atomic ratios of CeCu–SiC–Al_2O_3 and CeCu–SiC were 0.51 and 0.42, respectively. The high Ce^{3+}/Ce_{3d} atomic ratio on the CeCu–SiC–Al_2O_3 surface indicated high concentration of oxygen defects in the highly dispersed cerium oxide phase, which facilitated SO_3 decomposition. This finding may be attributed to the small size of the cerium oxide particles of CeCu–SiC–Al_2O_3 and large specific surface area[18].Owing to the boundary effect, the surface was likely to form defect sites in cerium oxide crystal. Figure 6 also shows the Cu_{2p} signal peaks in the XPS spectra of the CeCu–SiC–Al_2O_3 and CeCu–SiC catalysts. Sample peaks were observed near 962.5° and 941.9° with significantly vibrational peaks, and Cu elements were mostly Cu^{2+}.

Nitrogen adsorption test, TEM, XRD, and particle size analysis revealed that the carrier was a mesoporous structure and exhibited a strong interaction with the adsorbed mass. XPS analysis showed that the interaction between Al_2O_3 and SiC, as well as the uniform dispersion of cerium oxide, strengthened the SO_3 adsorption on the surface. Consequently, CeCu–SiC–Al_2O_3 activity would be reinforced by a large margin within the low temperature range. Therefore, SO_3 conversion was similar to the characterization results. SiC–Al_2O_3 was identified as the candidate support among the ones examined which exhibited the highest potential, which would be further verified in TPR.

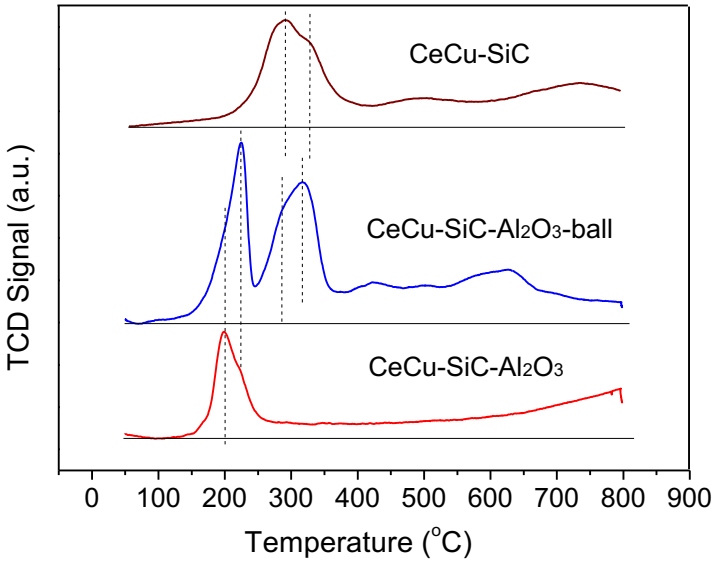

Figure 7. H_2–TPR profiles of catalysts CeCu–SiC,CeCu–SiC–Al_2O_3–ball,and CeCu–SiC–Al_2O_3.

TPR was conducted to investigate the structure of the catalysts and thus ascertain the nature of the surface species. The H_2–TPR profiles of the catalysts CeCu–SiC, CeCu–SiC–Al_2O_3, and CeCu–SiC–Al_2O_3 are depicted in Figure7.Reduction of the small CuO cluster and several adsorbed oxygen species occurred at 150°C–350°C[42]; that is, CuO was reduced to Cu_2O and then reduced to Cu. Reduction at 400°C–600°Cwas attributed to the relatively large CuO granule and ceria grain surface; at temperature >600°C,this occurrence was regarded as crystalline CeO_2 surface reduction[42]. CeCu–SiC–Al_2O_3 obtained the lowest reduction peak temperature at 150°C–350°C. The larger reduction peak that was gradually formed starting at 500 °C belonged to the CeO_2 particles. The decrease in the reduction temperature of CeO_2 to a low temperature indicated that CeO_2 had a small particle size, which was consistent with the XRD and TEM results. The CuO reduction temperature was the key indicator of the SO_3 decomposition mechanism[33], which indicated that CeCu–SiC–Al_2O_3 exhibited the highest catalytic activity. The reduction curves of CeCu–SiC composite oxide were divided into 3 distinct peaks. The peaks from low to high temperatures belonged to small CuO cluster particles and larger particle surface reduction, larger CuO granule reduction, and crystalline CeO_2 surface reduction. The CuO reduction peak in CeCu–SiC–Al_2O_3–ball was divided into 2 distinct separated peaks. The first peak at 150°C–250°C belonged to the smaller CuO granule, and the second peak at 250-350°C belonged to the larger CuO granule; the catalytic activity was also verified to be between the 2 previous samples. Moreover, the reduction peaks of the large CuO particles and CeO_2 on CeCu–SiC–Al_2O_3 and CeCu–SiC–Al_2O_3–ball moved in the low-temperature direction, compared with CeCu–SiC.

3.3.**Catalytic stability**

To determine the stability of CeCu–SiC–Al_2O_3, the catalyst was evaluated for 50 h under different space velocity conditions. Figure 8 shows that the catalytic activity decreases by about 10% for 20 h with 10 $g/g_{catalyst}$-h space velocity and then remained stable for 50 h. Therefore, SiC coating could prevent the aluminum sulfate formation even at 625°C[24]. At a space velocity of 50 $g/g_{catalyst}$-h, the initial catalytic activity was markedly reduced. The conversion ratio exhibited 18%, which dropped to 13% in the subsequent test that lasted for 35h. During the whole testing period, the catalytic activity remained relatively stable, indicating that the catalytic stability was satisfactory. At a space velocity of 10 $g/g_{catalyst}$-h, the activity decreased by 10 % for the first 20 h

and then remained almost the same for 50 h, which might be related to the decrease in the surface pore structure of the catalyst, as inferred from the TEM results in Figure 9.

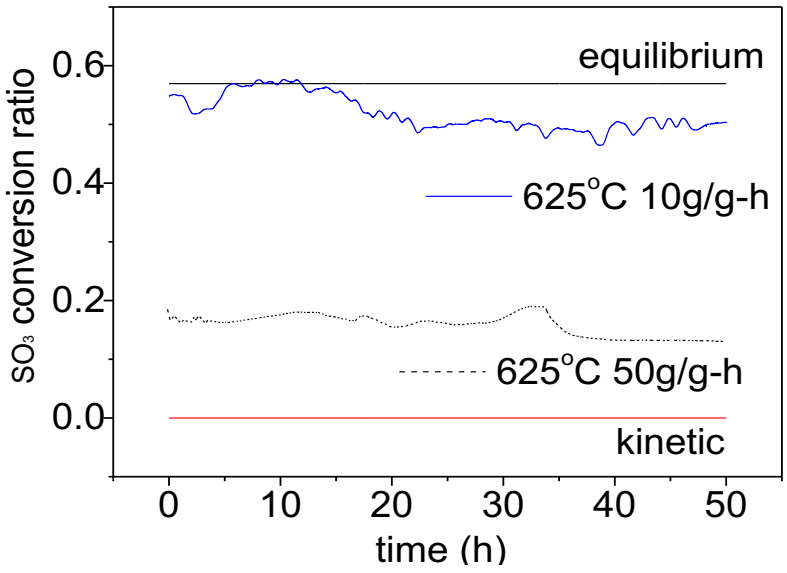

Figure 8. Stability test for CeCu–SiC–Al_2O_3 at 625°C for 50h.

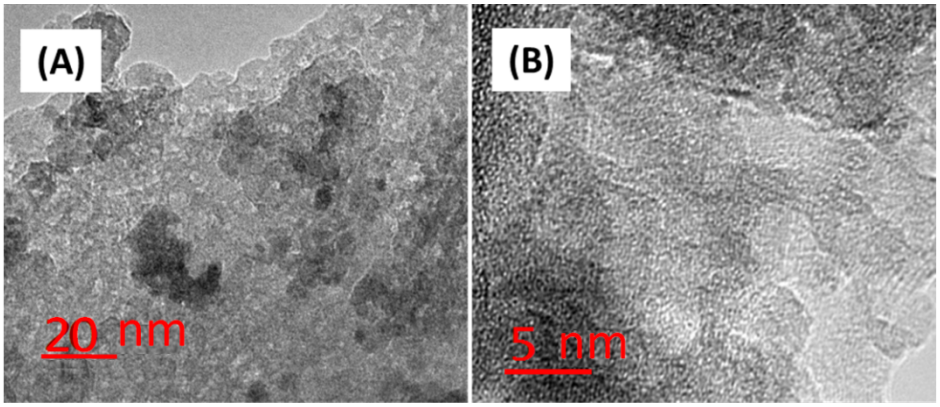

Figure 9. TEM results for CeCu–SiC–Al_2O_3 (A) before and (B) after the experiment.

4. Conclusion

In this study, the catalysts were prepared using carriers like SiC, Al_2O_3, SiC–Al_2O_3–ball, and SiC–Al_2O_3. SiC–Al_2O_3 was identified as the best catalyst carrier. CeCu‐SiC–Al_2O_3 was not significantly affected by the harsh reaction conditions at low temperatures. The SO_3 decomposition temperature was reduced to 625°C by CeCu‐SiC–Al_2O_3, 400°C less than the sulfuric acid homogeneous decomposition temperature. Compared with that of the catalyst CuO/CeO_2, the sulfuric acid decomposition temperature was reduced by about 200°C. As revealed by catalytic stability testingfor 50 h, the conversion rate was slightly decreased and stabilized at 50% or higher. However, with an increase in sulfuric acid flow rate, the catalytic conversion of SO_3 decreased significantly, and even the catalyst was temporarily deactivated at 625 °C.

The pore structure and adsorption properties of the 4 supported catalysts determined from N_2 adsorption and desorption tests indicated that SiC–Al_2O_3 was the most favorable material for adsorption. TEM (HRTEM) and XRD results showed that cerium–copper oxide was well dispersed and immobilized on the surface of the carriers, whereas the cerium–copper oxide on the

$SiC–Al_2O_3$ surface was more highly dispersed. XPS analysis showed that the $SiC–Al_2O_3$ surface, mainly consisted of Al_2O_3, SiC, and SiO_2.The atomic ratio of Ce^{3+}/Ce_{3d} in $SiC–Al_2O_3$ was higher than that in SiC, which indicated the presence of a large number of defective sites and higher SO_3 adsorption. In the H_2–TPR result, the CuO reduction temperature on the $SiC–Al_2O_3$ surface was also much lower than that on the SiC surface. Catalytic SO_3 decomposition testing indicated that $SiC–Al_2O_3$ was the best carrier for cerium copper oxide. The experimental results suggested that the $SiC–Al_2O_3$ preparation method could be applied to develop stable and active catalysts for SO_3 decomposition.

Acknowledgment

This work was supported by the National Natural Science Foundation of China (51621005) and the EPSRC research council from UK.

REFERENCES

[1] Dincer I. Environmental and sustainability aspects of hydrogen and fuel cell systems. International Journal of Energy Research. 2007;31:29-55.

[2] Dincer I, Balta MT. Potential thermochemical and hybrid cycles for nuclear‐based hydrogen production. International Journal of Energy Research. 2011;35:123-37.

[3] Giaconia A, Grena R, Lanchi M, Liberatore R, Tarquini P. Hydrogen/methanol production by sulfur–iodine thermochemical cycle powered by combined solar/fossil energy. International Journal of Hydrogen Energy. 2007;32:469-81.

[4] Kubo S, Nakajima H, Kasahara S, Higashi S, Masaki T, Abe H, et al. A demonstration study on a closed-cycle hydrogen production by the thermochemical water-splitting iodine–sulfur process. Nuclear Engineering and Design. 2004;233:347-54.

[5] Belaissaoui B, Thery R, Meyer XM, Meyer M, Gerbaud V, Joulia X. Vapour reactive distillation process for hydrogen production by HI decomposition from HI–I 2–H 2 O solutions. Chemical Engineering and Processing: Process Intensification. 2008;47:396-407.

[6] Favuzza P, Felici C, Lanchi M, Liberatore R, Mazzocchia C, Spadoni A, et al. Decomposition of hydrogen iodide in the S–I thermochemical cycle over Ni catalyst systems. International journal of hydrogen energy. 2009;34:4049-56.

[7] Petkovic LM, Ginosar DM, Rollins HW, Burch KC, Deiana C, Silva HS, et al. Activated carbon catalysts for the production of hydrogen via the sulfur–iodine thermochemical water splitting cycle. international journal of hydrogen energy. 2009;34:4057-64.

[8] Tyagi D, Varma S, Bharadwaj S. Pt/graphite catalyst for hydrogen generation by HI decomposition reaction in S–I thermochemical cycle. International Journal of Energy Research. 2015;39:2008-18.

[9] Wang L, Han Q, Li D, Wang Z, Chen J, Chen S, et al. Comparisons of Pt catalysts supported on active carbon, carbon molecular sieve, carbon nanotubes and graphite for HI decomposition at different temperature. International Journal of Hydrogen Energy. 2013;38:109-16.

[10] Zhang P, Su T, Chen Q, Wang L, Chen S, Xu J. Catalytic decomposition of sulfuric acid on composite oxides and Pt/SiC. international journal of hydrogen energy. 2012;37:760-4.

[11] Ying Z, Zhang Y, Xu S, Zhou J, Liu J, Wang Z, et al. Equilibrium potential for the electrochemical Bunsen reaction in the sulfur–iodine cycle. International Journal of Hydrogen Energy. 2014;39:18727-33.

[12] Ying Z, Zheng X, Cui G. Detailed kinetic study of the electrochemical Bunsen reaction in the

sulfur–iodine cycle for hydrogen production. Energy Conversion and Management. 2016;115:26-31.
[13] Ying Z, Zheng X, Zhang Y, Cui G. Development of a novel flowsheet for sulfur–iodine cycle based on the electrochemical Bunsen reaction for hydrogen production. International Journal of Hydrogen Energy. 2017;42:26586-96.
[14] Nadar A, Banerjee AM, Pai MR, Pai RV, Meena SS, Tewari R, et al. Catalytic properties of dispersed iron oxides Fe2O3/MO2 (M = Zr, Ce, Ti and Si) for sulfuric acid decomposition reaction: Role of support. International Journal of Hydrogen Energy. 2018;43:37-52.
[15] Singhania A, Bhaskarwar AN. TiO2 as a catalyst for hydrogen production from hydrogen-iodide in thermo-chemical water-splitting sulfur-iodine cycle. Fuel. 2018;221:393-8.
[16] Singhania A, Bhaskarwar AN. Effect of rare earth (RE – La, Pr, Nd) metal-doped ceria nanoparticles on catalytic hydrogen iodide decomposition for hydrogen production. International Journal of Hydrogen Energy. 2018;43:4818-25.
[17] Singhania A, Krishnan VV, Bhaskarwar AN, Bhargava B, Parvatalu D. Hydrogen-iodide decomposition over PdCeO2 nanocatalyst for hydrogen production in sulfur-iodine thermochemical cycle. International Journal of Hydrogen Energy. 2018;43:3886-91.
[18] Yang H, Zhang Y, Zhou J, Wang Z, Liu J, Cen K. Study on CuO–CeO2/SiC catalysts in the sulfur–iodine cycle for hydrogen production. International Journal of Energy Research. 2016.
[19] Schwartz D, Gadiou R, Brilhac JB, Prado G, Martinez G. A kinetic study of the decomposition of spent sulfuric acids at high temperature. Industrial & Engineering Chemistry Research. 2000;39:2183-9.
[20] Zhang YW, Yang H, Zhou JH, Wang ZH, Liu JZ, Cen KF. Detailed kinetic modeling of homogeneous H2SO4 decomposition in the sulfur-iodine cycle for hydrogen production. Appl Energ. 2014;130:396-402.
[21] Barbarossa V, Brutti S, Diamanti M, Sau S, De Maria G. Catalytic thermal decomposition of sulphuric acid in sulphur–iodine cycle for hydrogen production. International journal of hydrogen energy. 2006;31:883-90.
[22] Brutti S, De Maria G, Cerri G, Giovannelli A, Brunetti B, Cafarelli P, et al. Decomposition of H2SO4 by direct solar radiation. Industrial & Engineering Chemistry Research. 2007;46:6393-400.
[23] Norman J, Sharp R, Williamson D, Mysels K. Studies of the sulfur-iodine thermochemical water-splitting cycle. Hydrogen Energy Progress1981. p. 257-75.
[24] Lee SY, Jung H, Kim WJ, Shul YG, Jung K-D. Sulfuric acid decomposition on Pt/SiC-coated-alumina catalysts for SI cycle hydrogen production. International Journal of Hydrogen Energy. 2013;38:6205-9.
[25] Giaconia A, Sau S, Felici C, Tarquini P, Karagiannakis G, Pagkoura C, et al. Hydrogen production via sulfur-based thermochemical cycles: Part 2: Performance evaluation of Fe2O3-based catalysts for the sulfuric acid decomposition step. International Journal Of Hydrogen Energy. 2011;36:6496-509.
[26] Banerjee AM, Shirole AR, Pai MR, Tripathi AK, Bharadwaj SR, Das D, et al. Catalytic activities of Fe2O3 and chromium doped Fe2O3 for sulfuric acid decomposition reaction in an integrated boiler, preheater, and catalytic decomposer. Applied Catalysis B-Environmental. 2012;127:36-46.
[27] Kawada T, Hinokuma S, Machida M. Structure and SO3 decomposition activity of nCuO-V2O5/SiO2 (n=0, 1, 2, 3 and 5) catalysts for solar thermochemical water splitting cycles. Catalysis Today. 2015;242:268-73.
[28] Machida M, Kawada T, Hebishima S, Hinokuma S, Takeshima S. Macroporous Supported Cu-V Oxide as a Promising Substitute of the Pt Catalyst for Sulfuric Acid Decomposition in Solar Thermochemical Hydrogen Production. Chemistry Of Materials. 2012;24:557-61.

[29] Machida M, Kawada T, Yamashita H, Tajiri T. Role of Oxygen Vacancies in Catalytic SO3 Decomposition over Cu2V2O7 in Solar Thermochemical Water Splitting Cycles. Journal Of Physical Chemistry C. 2013;117:26710-5.
[30] Kawada T, Hinokuma S, Machida M. Structure and SO 3 decomposition activity of nCuO–V 2 O 5/SiO 2 (n= 0, 1, 2, 3 and 5) catalysts for solar thermochemical water splitting cycles. Catalysis Today. 2015;242:268-73.
[31] Kawada T, Yamashita H, Zheng Q, Machida M. Hydrothermal synthesis of CuV 2 O 6 supported on mesoporous SiO 2 as SO 3 decomposition catalysts for solar thermochemical hydrogen production. International Journal of Hydrogen Energy. 2014;39:20646-51.
[32] Machida M, Kawada T, Yamashita H, Tajiri T. Role of oxygen vacancies in catalytic SO3 decomposition over Cu2V2O7 in solar thermochemical water splitting cycles. The Journal of Physical Chemistry C. 2013;117:26710-5.
[33] Zhang Y, Yang H, Zhou J, Wang Z, Liu J, Cen K. Catalytic decomposition of sulfuric acid over CuO/CeO 2 in the sulfur–iodine cycle for hydrogen production. International Journal of Hydrogen Energy. 2015;40:2099-106.
[34] Kim T-H, Gong G-T, Lee BG, Lee K-Y, Jeon H-Y, Shin C-H, et al. Catalytic decomposition of sulfur trioxide on the binary metal oxide catalysts of Fe/Al and Fe/Ti. Applied Catalysis A: General. 2006;305:39-45.
[35] Ginosar DM, Petkovic LM, Glenn AW, Burch KC. Stability of supported platinum sulfuric acid decomposition catalysts for use in thermochemical water splitting cycles. International Journal of Hydrogen Energy. 2007;32:482-8.
[36] Noh S-C, Lee SY, Shul YG, Jung K-D. Sulfuric acid decomposition on the Pt/n-SiC catalyst for SI cycle to produce hydrogen. International Journal of Hydrogen Energy. 2014;39:4181-8.
[37] Rajendran A, Takahashi Y, Koyama M, Kubo M, Miyamoto A. Tight-binding quantum chemical molecular dynamics simulation of mechano-chemical reactions during chemical–mechanical polishing process of SiO 2 surface by CeO 2 particle. Applied Surface Science. 2005;244:34-8.
[38] Ungár T, Gubicza J, Hanák P, Alexandrov I. Densities and character of dislocations and size-distribution of subgrains in deformed metals by X-ray diffraction profile analysis. Materials Science and Engineering: A. 2001;319:274-8.
[39] Dauscher A, Hilaire L, Le Normand F, Müller W, Maire G, Vasquez A. Characterization by XPS and XAS of supported Pt/TiO2 CeO2 catalysts. Surface and Interface Analysis. 1990;16:341-6.
[40] Kibel MH, Leech PW. X-ray photoelectron spectroscopy study of optical waveguide glasses. Surface and interface analysis. 1996;24:605-10.
[41] Niesz K, Morse DE. Sonication-accelerated catalytic synthesis of oxide nanoparticles. Nano Today. 2010;5:99-105.
[42] Martínez-Arias A, Gamarra D, Fernández-García M, Hornés A, Bera P, Koppány Z, et al. Redox-catalytic correlations in oxidised copper-ceria CO-PROX catalysts. Catalysis Today. 2009;143:211-7.